Numerical investigation of cosmological singularities

Beverly K. Berger*
Institute for Theoretical Physics, University of California, Santa Barbara, California 93106
and Physics Department, Oakland University, Rochester, Michigan 48309

Vincent Moncrief†
Institute for Theoretical Physics, University of California, Santa Barbara, California 93106
and Department of Physics, Yale University, New Haven, Connecticut 06511
(Received 26 July 1993)

Although cosmological solutions to Einstein's equations are known to be generically singular, little is known about the nature of singularities in typical spacetimes. It is shown here how the operator splitting used in a particular symplectic numerical integration scheme fits naturally into the Einstein equations for a large class of cosmological models (whose dynamical variables are harmonic maps) and thus allows the study of their approach to the singularity. The numerical method also naturally singles out the asymptotically velocity term dominated (AVTD) behavior known to be characteristic of some of these models, conjectured to describe others, and probably characteristic of a subclass of the rest. The method is first applied to the generic (unpolarized) Gowdy T^3 cosmology. Exact pseudounpolarized solutions are used as a code test and demonstrate that a fourth-order accurate implementation of the numerical method yields acceptable agreement. For generic initial data, support for the conjecture that the singularity is AVTD with geodesic velocity (in the harmonic map target space) <1 is found. A new phenomenon of the development of small scale spatial structure is also observed. Finally, it is shown that the numerical method straightforwardly generalizes to an arbitrary cosmological spacetime on $T^3 \times R$ with one spacelike U(1) symmetry.

PACS number(s): 04.20.Jb, 04.30.+x, 98.80.Hw

I. INTRODUCTION

Powerful theorems [1] prove singularities to be a generic feature of Einstein's equations yet say nothing about the nature of these singularities. In particular, little is known about the singularity behavior of generic spatially inhomogeneous cosmologies. Belinskii, Khalatnikov, and Lifshitz (BKL) [2] and co-workers [3] have long argued that the mixmaster dynamics [2,4] of spatially homogeneous Bianchi type-VIII and -IX cosmologies [5] characterizes the generic "Big Bang." Their results are not generally accepted, however [6], and evidence suggests that mixmaster behavior disappears in models with more than three dynamical degrees of freedom [7]. An alternative to mixmaster dynamics is asymptotically velocity term dominated (AVTD) behavior where (heuristically) terms in Einstein's equations containing spatial derivatives can be neglected in favor of those with time derivatives [8,9]. Near the singularity, AVTD solutions can be interpreted as a different spatially homogeneous cosmology at each point in space. The polarized Gowdy cosmologies [10] have been shown rigorously to belong to this class [9,11,12]. It has recently been conjectured that the general (unpolarized) Gowdy models are AVTD [13].

We propose to study the approach to the singularity numerically using a method uniquely suited to the task. For both the Gowdy cosmologies defined to have a symmetry plane (i.e., two spatial, hypersurface-orthogonal, surface-forming Killing fields) and the more general cosmology possessing a single, spatial U(1) symmetry [14] (at least some of the) degrees of freedom can be understood as harmonic maps [15]. The super-Hamiltonian whose variation yields these equations is just an energy-like expression of the harmonic map fields [16]. The variation of the "kinetic" term alone yields the AVTD equations of motion for these fields (with all spatial-derivative-containing terms obtained upon variation of the "potential" term). This suggests that a symplectic scheme for numerical integration that separately evolves the kinetic and potential energy operators to approximate the total Hamiltonian evolution is ideally suited to this problem [17]. In the following discussion, we shall demonstrate that this is indeed the case.

The approach to the singularity of the Gowdy T^3 cosmology has been used to test the feasibility of our approach. In the process of code development and testing, we have been able to demonstrate AVTD behavior of the singularity approach for several sets of (presumably) generic initial data. We have also noted that the solutions develop a characteristic small-scale spatial structure which represents a competition between nonlinear growth and the approach to the AVTD regime which freezes the spatial profile of the wave amplitudes. This richness of the Gowdy T^3 phenomenology will be discussed elsewhere [18]. Here we wish to emphasize the applicability of our methods to the study of cosmological singularities.

*Electronic address: berger@vela.acs.oakland.edu
†Electronic address: moncrief@yalph2.bitnet

While the numerical study of plane symmetric cosmologies has been underway since the late 1970s [19], previous work tended to focus on analogies between the cosmological problem and the original numerical studies of colliding black holes [20]. This led to concentration on constant mean curvature foliations and on the choice of lapse and shift. Physical interest centered on interacting wave packets of a single polarization. In contrast, we begin with the predefined coordinate system in which the equations are known to be relatively simple and within which the harmonic map structure can be seen. This foliation naturally selects (in the plane symmetric case) a measure of area in the symmetry plane as the time variable. Our approach then easily allows the study of unpolarized Gowdy T^3 models and appears to be generalizable to the U(1) problem.

In Sec. II, we shall describe the numerical method including its generalization to arbitrary order of accuracy in both time [21] and space. To date, our primary application of this method has been to the approach to the singularity of the unpolarized Gowdy T^3 cosmology [10,12,16,22]. In Sec. III, the relevant properties of this model will be reviewed. Section IV demonstrates the validity of the code with a "pseudounpolarized" test model constructed by boosting in the harmonic map target space an analytic solution for the polarized model. In Sec. V, we discuss results for a generic unpolarized model, demonstrating AVTD behavior and briefly discussing the appearance of small-scale spatial structure. In Sec. VI, the applicability of this method to the U(1) problem is shown. A summary and conclusions are given in Sec. VII.

II. THE SYMPLECTIC INTEGRATOR (SI) [17]

For convenience, we shall restrict our discussion of the method to a single degree of freedom which depends on only one spatial dimension and time—$q(x,t)$ and its conjugate momentum $\pi(x,t)$. We assume that the equations of motion can be obtained by variation of a Hamiltonian:

$$H=\oint dx\,[\tfrac{1}{2}\pi^2+V(q)]\ . \tag{2.1}$$

Consider a differenced form of (2.1):

$$H=\sum_{i=0}^{N}[\tfrac{1}{2}(\pi_i^j)^2+V_i(q_k^j)]\ , \tag{2.2}$$

where we assume periodic boundary conditions on the lattice with labels (i,j) denoting the point (x_i,t^j). The potential V_i at the point x_i may depend on the value of q at several spatial grid points.

The symplectic scheme splits the Hamiltonian operator as

$$H=H_1+H_2\ , \tag{2.3}$$

where

$$H_1=\oint dx\tfrac{1}{2}\pi^2 \tag{2.4a}$$

and

$$H_2=\oint dx\ V(q)\ , \tag{2.4b}$$

respectively. It is convenient to represent the scheme using quantum mechanical notation. It is based on the second-order (in the time step ε) accurate approximant to the evolution operator:

$$e^{-i\varepsilon H}=e^{-(i/2)\varepsilon H_2}e^{-i\varepsilon H_1}e^{-(i/2)\varepsilon H_2}+O(\varepsilon^3)\ , \tag{2.5}$$

i.e., to evolve (π_i^j,q_i^j) at (x_i,t^j) to (π_i^{j+1},q_i^{j+1}) at $(x_i,t^j+\varepsilon)$, evolve with H_2 for a $\frac{1}{2}$ time step, with H_1 for a full time step, and with H_2 for a $\frac{1}{2}$ time step using the appropriate intermediate result at each stage. In this evolution, H_1 and H_2 are separately to be regarded as the Hamiltonian of the system. In the case where H_1 and H_2 can be separately exactly solved, the implementation of the method becomes trivial.

For the Hamiltonian (2.1), the scheme becomes [17]

$$\begin{aligned} q_i^{j+1}&=q_i^j+\varepsilon[\pi_i^j+\tfrac{1}{2}\varepsilon F_i(q_k^j)]\ ,\\ \pi_i^{j+1}&=\pi_i^j+\tfrac{1}{2}\varepsilon F_i(q_k^j)+\tfrac{1}{2}\varepsilon F_i(q_k^{j+1})\ , \end{aligned} \tag{2.6}$$

where $F_i(q_k^j)=-\partial V/\partial q_i^j$ is the appropriate force component. As an example, we consider the wave equation with

$$H_2=\sum_{i=0}^{N}\frac{1}{2\Delta^2}(q_{i+1}^j-q_i^j)^2\ , \tag{2.7}$$

where Δ is the lattice spacing in the x direction. Direct substitution shows that, in this case, the method is equivalent to the standard leap-frog differenced form of the wave equation [23]:

$$q_i^{j+1}+q_i^{j-1}-q_{i+1}^j-q_{i-1}^j=0\ . \tag{2.8}$$

However, the SI algorithm has significant advantages over the leap-frog scheme for our problem of the approach to the singularity.

(1) As a symplectic scheme, the evolution takes the form of a canonical transformation from the beginning to the end of the time step [17]. This may help to preserve the constraints of the cosmological problem during the evolution. (Although the continuum Einstein equations automatically preserve the constraints during evolution, there is no corresponding statement for the discretized equations. Ultimately, this is a consequence of the role of the constraints as the generators of diffeomorphism invariance—a fundamental property of the continuum.)

(2) In the cosmological case, H_1 is the Hamiltonian whose variation yields the AVTD equations. If the solution is in the AVTD regime, then this SI will become increasingly more accurate.

(3) To avoid the problematic need to solve and resolve the constraint equations at frequent intervals [24,20], one can try to find an accurate solution to the dynamical equations. Suzuki has shown how to generalize the SI to an arbitrary order in time [21]. The idea is to find an approximant such as (2.5), accurate to the desired order. Such a program does not have a unique solution. Since it can be shown [21] that a $(2m-1)$-order accurate scheme is also $2m$-order accurate, one finds the recurrence relation [21]

$$S_{2m-1}(\varepsilon)=S_{2m}(\varepsilon)$$
$$=S_{2m-3}(k_m\varepsilon)S_{2m-3}[(1-2k_m)\varepsilon]$$
$$\times S_{2m-3}(k_m\varepsilon)\ , \tag{2.9}$$

where

$$k_m=(2-2^{1/(2m-1)})^{-1} \tag{2.10}$$

with

$$S_1(\varepsilon)=e^{-(i/2)\varepsilon H_2}e^{-i\varepsilon H_1}e^{-(i/2)\varepsilon H_2}\ . \tag{2.11}$$

Thus, the higher-order scheme can be constructed from time steps of the appropriate duration of the second-order scheme.

The generalization of the spatial evolution to arbitrary order is simple only for one spatial dimension. For higher dimensions, the construction must proceed on a case by case basis. In the one spatial dimension wave equation, the second derivative with respect to x can be obtained in a differenced form (for spatial grid interval Δ) as

$$\frac{d^2f}{dq^2}=a_nf(q_i)+\frac{1}{\Delta^2}\sum_{k=1}^{n-1}a_k[f(q_i+k\Delta)+f(q_i-k\Delta)]$$
$$+O(\Delta^{2n})\ . \tag{2.12}$$

The coefficients are chosen to cancel the terms in the Taylor expression containing higher derivatives to the indicated order. The expression on the right-hand side of (2.12) can be obtained as the negative of the variation with respect to f_i [where $f_i\equiv f(q_i)$] of

$$V=\sum_{i=0}^{N}\sum_{k=1}^{n-1}\frac{a_k}{2\Delta^2}(f_{i+k}-f_i)^2\ , \tag{2.13}$$

where the coefficients a_k are the same as those in (2.12) and with $a_n=-2\sum_{k=1}^{n-1}a_k$. Thus, the second-order accurate expression is (2.7) with the fourth-order accurate one given by

$$V=\sum_{i=0}^{N}\left[\frac{2}{3\Delta^2}(q_{i+1}-q_i)^2-\frac{1}{24\Delta^2}(q_{i+2}-q_i)^2\right]\ , \tag{2.14}$$

etc. This prescription is easily extended to more general potentials; e.g.,

$$V=\oint dx\tfrac{1}{2}F(q)q^2 \tag{2.15}$$

is differenced as

$$V=\sum_{i=0}^{N}\sum_{k=1}^{n-1}\frac{a_k}{2}F[\tfrac{1}{2}(q_{i+k}+q_i)](q_{i+k}-q_i)^2\ . \tag{2.16}$$

For two spatial dimensions, generalization to the Laplacian is trivial. However, potentials with cross terms or different coefficients for $\partial^2/\partial x^2$ and $\partial^2/\partial y^2$ cannot be differenced to higher order by this prescription due to the difficulty of eliminating higher derivative terms in a multidimensional Taylor expansion.

III. THE GOWDY T^3 UNIVERSE TEST CASE

The Gowdy T^3 cosmology is conveniently described by the metric [16]

$$ds^2=e^{\lambda/2}e^{\tau/2}(-e^{-2\tau}d\tau^2+d\theta^2)$$
$$+e^{-\tau}[e^Pd\sigma^2+2e^PQd\sigma\,d\delta+(e^PQ^2+e^{-P})d\delta^2]\ , \tag{3.1}$$

where λ, P, and Q are functions of θ and τ only. The T^3 spatial topology is imposed by requiring the angular coordinates σ and δ to have arbitrary finite range and $0\le\theta\le2\pi$. The time variable τ measures the area in the symmetry plane and $\to\infty$ at the singularity [9,12]. The physical interpretation of the polarized model ($Q\equiv0$) has been discussed extensively [12,25]. The independent Einstein equations from (3.1) are

$$P_{,\tau\tau}-e^{-2\tau}P_{,\theta\theta}-e^{2P}(Q_{,\tau}^2-e^{-2\tau}Q_{,\theta}^2)=0\ , \tag{3.2}$$

$$Q_{,\tau\tau}-e^{-2\tau}Q_{,\theta\theta}+2(P_{,\tau}Q_{,\tau}-e^{-2\tau}P_{,\theta}Q_{,\theta})=0\ , \tag{3.3}$$

$$\lambda_{,\theta}-2(P_{,\theta}P_{,\tau}+e^{2P}Q_{,\theta}Q_{,\tau})=0\ , \tag{3.4}$$

and

$$\lambda_{,\tau}-[P_{,\tau}^2+e^{-2\tau}P_{,\theta}^2+e^{2P}(Q_{,\tau}^2+e^{-2\tau}Q_{,\theta}^2)]=0\ . \tag{3.5}$$

The latter two equations for the background $\lambda(\theta,\tau)$ are, respectively, the θ momentum and Hamiltonian constraints. [The T^3 topology requires the integral of (3.4) to vanish—equivalent to requiring zero total θ momentum.]

Since the "wave" equations (3.2) and (3.3) do not contain λ, their evolution is unconstrained. It has been shown, albeit for a different set of variables defined by [16]

$$e^P=\cosh W+\sinh W\cos\Phi\ ,$$
$$e^PQ=\sinh W\sin\Phi\ , \tag{3.6}$$

that the "wave" equations are harmonic map equations for the metric:

$$dS^2=dP^2+e^{2P}dQ^2\ . \tag{3.7}$$

This is just the harmonic map property of the fields P and Q with (3.7) the metric of the target space [15]. The field equations can then be derived from the Hamiltonian

$$H=\frac{1}{2}\oint d\theta[\pi_P^2+e^{-2P}\pi_Q^2+e^{-2\tau}(P_{,\theta}^2+e^{2P}Q_{,\theta}^2)]\ . \tag{3.8}$$

Clearly, (3.8) is in the form required by the SI algorithm.

We note here for future references that the metric (3.7) admits three Killing fields corresponding to the transformations (for constant parameter ρ)

$$\{P\to P,$$
$$Q\to Q+\rho\}\ , \tag{3.9}$$

$$\{P\to P-\ln\rho,$$
$$Q\to\rho Q\}\ , \tag{3.10}$$

and

$$\{e^P \to \tfrac{1}{2}[e^P(1+Q^2)+e^{-P}] + \tfrac{1}{2}[e^P(1-Q^2)-e^{-P}]\cos\rho - e^P Q \sin\rho \ , \quad e^P Q \to e^P Q \cos\rho + \tfrac{1}{2}[e^P(1-Q^2)-e^{-P}]\sin\rho\} \ . \tag{3.11}$$

This last apparently complicated transformation is just $W \to W$, $\Phi \to \Phi + \Phi_0$ in the other coordinates. The presence of the factor $e^{-2\tau}$ in (3.8) and in the wave equations suggests that as the singularity at $\tau = \infty$ is approached, the spatial derivatives can be neglected yielding the AVTD solution. In the absence of the spatial derivative terms, Eqs. (3.2) and (3.3) can be solved exactly in terms of four arbitrary constants α, β, ζ, and ξ as

$$P = \ln[\alpha e^{-\beta\tau}(1+\zeta^2 e^{2\beta\tau})] \tag{3.12}$$

and

$$Q = -\frac{\zeta e^{2\beta\tau}}{\alpha(1+\zeta^2 e^{2\beta\tau})} + \xi \ . \tag{3.13}$$

Substitution of (3.12) and (3.13) into the AVTD form of (3.4) and (3.5) yields

$$\lambda = -\beta^2\tau + \lambda_0 \ . \tag{3.14}$$

As $\tau \to \infty$, (3.12) and (3.13) become

$$P = \beta\tau, \quad Q = Q_0 \ , \tag{3.15}$$

with $Q_0 = 1/\alpha\zeta + \xi$. If a Gowdy solution approaches the AVTD limit, one expects it to have the form (3.12)–(3.14) with (in general) different values of α, β, ζ, and ξ at each value of θ. For the polarized case ($Q=0$), it was shown [12] that substitution of (3.15) as the limiting form of the exact solution in the metric (3.1) yields the Kasner solution [26] with a θ-dependent Kasner parameter. In the general case ($Q \neq 0$), the Kasner axes are rotated with respect to the coordinate axes. Isenberg and Moncrief have shown [9] in the polarized case that every solution is AVTD. It is conjectured [13] that this is also true in the unpolarized model.

In the following discussion, we shall consider only the wave equations (3.2) and (3.3) since the background $\lambda(\theta,\tau)$ may be easily constructed after the dynamical P and Q have been found. That P and Q are amplitudes for the two orthogonal polarizations of gravitational waves may be seen by analogy with linearized gravity [12,27]. If the metric $g_{\mu\nu}$ is expressed as

$$g_{\mu\nu} = \gamma^{(0)}_{\mu\nu} + h^{(1)}_{\mu\nu} + k^{(2)}_{\mu\nu} \tag{3.16}$$

with P and Q assumed small then

$$\gamma^{(0)}_{\mu\nu} = \mathrm{diag}(-e^{\lambda/2}e^{-3\tau/2}, e^{\lambda/2}e^{\tau/2}, e^{-\tau}, e^{-\tau}) \tag{3.17a}$$

describes a background metric. The designation as background can be enhanced by the introduction of spatial averaging [27,28,25]. We also find that

$$h^{(1)}_{\mu\nu} = e^{-\tau}P\varepsilon_{+\mu\nu} + e^{-\tau}Q\varepsilon_{\times\mu\nu} \ , \tag{3.17b}$$

where ε_+ and $\varepsilon_\times$ are the gravitational wave polarization tensors. In the σ-δ plane,

$$k^{(2)}_{\mu\nu} = e^{-\tau}\begin{bmatrix} \frac{1}{2}P^2 & PQ \\ PQ & Q^2+\frac{1}{2}P^2 \end{bmatrix} \tag{3.17c}$$

with all other components zero. It is easy to see [12,27] that, in zeroth order, the waves act as sources for the background in Eqs. (3.4) and (3.5). In first order, P and Q satisfy linear wave equations (3.2) and (3.3). The nonlinearities of the waves enter at the next order. In some sense, we cannot consider these terms to be higher order since the solution is qualitatively different if both polarizations are present even if the amplitude of Q is small [29]. This is explained by the scaling symmetry (3.10) which implies that a solution to (3.2) and (3.3) is independent of the amplitude of Q as long as it is nonzero.

The polarized case (e.g., $Q=0$) yields a single linear wave equation with the general exact solution [12]

$$P(\theta,\tau) = \sum_{n=0}^{\infty} Z_0(ne^{-\tau})(a_n \cos n\theta + b_n \sin n\theta) \ , \tag{3.18}$$

where $Z_0(x)$ is a general solution to Bessel's equation of zero order and the a's and b's are arbitrary constants. It is possible to use this exact solution to generate exact "pseudounpolarized" solutions to the unpolarized equations (3.2) and (3.3) by means of the boost symmetry (3.11). Given an exact solution P_0 from (3.18), we obtain a class of solutions:

$$e^P = \cosh P_0 + \sinh P_0 \cos\rho \ , \quad e^P Q = \sinh P_0 \sin\rho \ , \tag{3.19}$$

for all values of the parameter $0 \le \rho \le 2\pi$. Perhaps the simplest of these solutions is

$$P = \ln\cosh P_0 \ , \quad Q = \tanh P_0 \ , \tag{3.20}$$

found for $\rho = \pi/2$. The pseudounpolarized solutions make excellent code tests since the fact that they are nongeneric is not apparent to the computer. Direct substitution of (3.20) into the equations of motion (3.2) and (3.3) shows that nonlinear terms from variation of both H_1 and H_2 [see the discussion in Sec. II and Eq. (3.8)] must cancel corresponding expressions which arise in the linear terms. Thus the entire code is tested.

Grubišić and Moncrief [13] have defined several functions of P and Q and their conjugate momenta which become constant in τ in the AVTD regime. They also predict the rate of decay to the AVTD regime in terms of the θ-dependent parameters α, β, ζ, and ξ. For the purposes of this paper, we shall consider only the parameter

$$v \equiv (P_{,\tau}^2 + e^{2P}Q_{,\tau}^2)^{1/2} \tag{3.21}$$

which represents geodesic velocity in the target space (3.7). Grubišić and Moncrief have conjectured that for a generic Gowdy T^3 model, the AVTD regime will be characterized by $0 \le v < 1$ for all θ. The restriction to

generic models must be made because any value of v is allowed for polarized solutions [9] and $v=1$ is achieved for some nonpolarized but "asymptotically polarized" solutions [30]. [We note that v is invariant under the transformations (3.9)–(3.11) so that pseudounpolarized solutions can also have any value of v.] The heuristic basis for this conjecture is easily seen. The term $e^{-2\tau}e^{2P}Q_{,\theta}^2$ in (3.2) becomes $e^{-2\tau(1-v)}Q_{,\theta}^2$ in the AVTD limit. Clearly, if $v>1$ (with $Q_{,\theta}$ fixed), this term will grow, contrary to the AVTD assumption that it is negligible.

IV. THE PSEUDOUNPOLARIZED TEST CASE

In differenced form, the Hamiltonian (3.8) becomes

$$H=\frac{1}{2}\sum_{i=1}^{N}(\pi_{P_i}^2+e^{-2P_i}\pi_{Q_i}^2)+\frac{e^{-2\tau}}{(\Delta\theta)^2}\sum_{i=0}^{N}\{a[(P_i-P_{i-1})^2+e^{P_i+P_{i-1}}(Q_i-Q_{i-1})^2]$$
$$+b[(P_i-P_{i-2})^2+e^{P_i+P_{i-2}}(Q_i-Q_{i-2})^2]\}\ , \tag{4.1}$$

where $(a,b)=(\frac{1}{2},0)$ and $(\frac{2}{3},-\frac{1}{24})$ yields equations correct to second and fourth orders, respectively, in the spatial derivatives. [Extension to sixth order requires corresponding terms $(P_{i+3}-P_i)^2$, etc., with coefficients $(a,b,c,)=(\frac{3}{4},-\frac{3}{40},\frac{1}{180})$.] The first sum is H_1 and the second H_2. To evolve with H_1, solve the AVTD solution [(3.12), (3.13), and their τ derivatives] for a given P and Q and their conjugate momenta (at each θ value) for the parameters α, β, ζ, and ξ. Use these parameters to propagate the initial data to the end of the time step. The evolution with H_2 is even easier since it contains no momenta so that P_i and Q_i remain constant. The momenta are evolved with the (now constant) gradients of H_2. The overall time-dependent factor $e^{-2\tau}$ is then trivially integrated. (We note that one may alternatively treat τ as an extra degree of freedom.) Suzuki's method [21] is used to ensure that the time evolution is accurate to the desired order. Greater details of our algorithm are given in the Appendix.

As a code test, initial data appropriate to the pseudounpolarized boost (3.20) of the exact solution to (3.18) given by

$$P_0(\theta,\tau)=Y_0(e^{-\tau})\cos\theta\ , \tag{4.2}$$

where $Y_0(x)$ is an irregular Bessel function, were evolved numerically toward the singularity [31]. The exact boosted solution is displayed in Fig. 1. Note that the boost transformation has generated large θ derivatives (particularly in Q) due to the hyperbolic tangent. Figures 2 and 3 illustrate the differences between the numerical and exact solutions for the second- and fourth-order schemes, respectively. Although the errors in the second-order algorithm are small almost everywhere ($\approx 1\%$), they become unacceptably large (≈ 1) as τ increases in the regions of large θ derivative. Improvement with the fourth-order scheme is dramatic with relative errors $\approx 10^{-5}$ everywhere.

The accuracy of the fourth-order code appears to be acceptable for the following reasons: The code tests were run with low spatial resolution of 100 total grid points with 99 (97) representing $[0,2\pi]$ for second (fourth) order (due to the imposition of periodic boundary conditions). The range of τ was between 0 and ≈ 23. The τ interval was chosen for convenience—there was no barrier to a much closer approach to the singularity. The large spatial gradients (in Q) were correctly represented by the code. We shall see (next section) that such features are, in fact, also characteristic of the generic Gowdy T^3 solution.

V. RESULTS FOR A "GENERIC" UNPOLARIZED GOWDY T^3 MODEL

Here we shall discuss the results from a single initial Gowdy T^3 data set for evolution toward the singularity. Comparison to other sets appears to indicate that the behavior we report here is typical for standing wave initial data. Traveling waves will be discussed elsewhere as will the full range of Gowdy T^3 phenomenology [18]. Following a suggestion by Chrusciel [32], we consider initial data for which the parameter v in (3.20) exceeds unity with the initial time dependence that of the AVTD

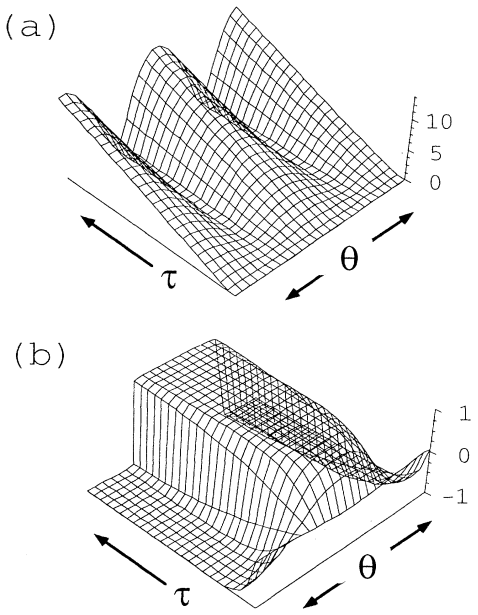

FIG. 1. The exact solution for the pseudounpolarized test case. Initial data are generated from Eq. (3.20) applied to (4.2) (and its τ derivative) evaluated at $\tau=0$. The axis scales for θ and τ are $[0,2\pi]$ and $[0,23]$, respectively. The vertical axis indicates the values of (a) $P(\theta,\tau)$ and (b) $Q(\theta,\tau)$.

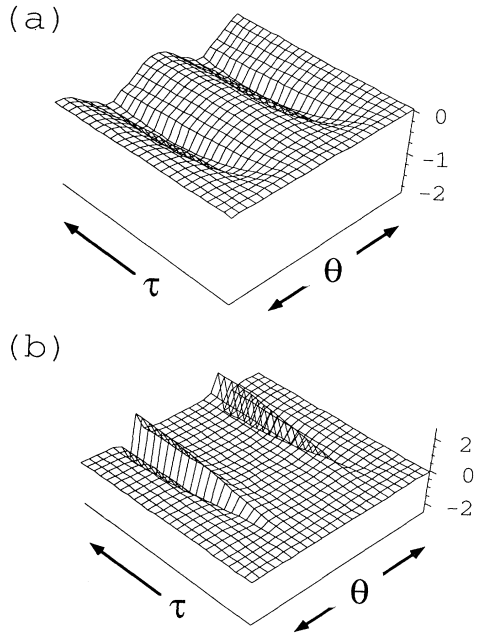

FIG. 2. Errors in the θ-τ plane for the second-order accurate numerical scheme. The ranges of θ and τ are the same as in Fig. 1. (a) The vertical scale measures $P_{\text{numerical}} - P_{\text{exact}}$ [where P_{exact} is shown in Fig. 1(a)] and $P_{\text{numerical}}$ is the computation. (b) The same as (a) but for Q.

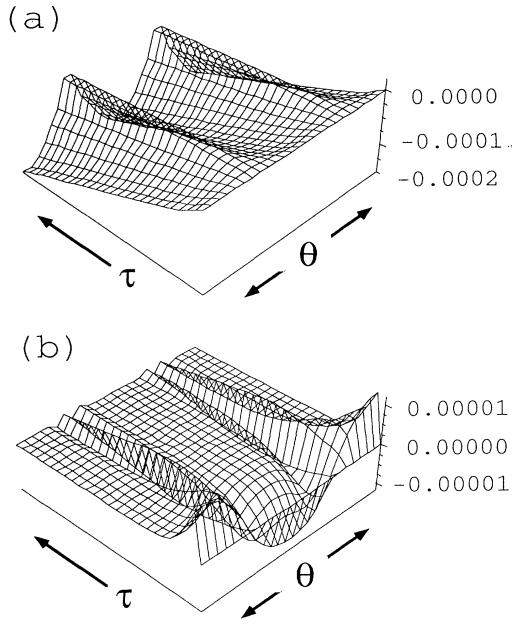

FIG. 3. Errors in the θ-τ plane for the fourth-order accurate numerical scheme. All axes and variables are the same as in Fig. 2 except that the fourth-order accurate numerical scheme has been used.

behavior (3.15). The conjecture [13] is that a true AVTD regime with $v < 1$ everywhere will arise during the course of the evolution. The selected initial data were

$$P = 0, \quad \pi_P = 10\cos\theta, \quad Q = \cos\theta, \quad \pi_Q = 0, \tag{5.1}$$

so that $v_0 = 10|\cos\theta|$. The evolution was performed with 800 spatial grid points for the range $0 \le \tau \le 6\pi$ with the fourth-order accurate code. To study the approach to the AVTD regime, we average reported (i.e., saved rather than computed) values of P, Q, and v over nearest and next-nearest neighbors (to avoid grid scale size structures which must be regarded to be unreliable). Figures 4–6 illustrate P, Q, and v, respectively, vs θ for various values of τ. The approach to the limiting AVTD behavior (3.15) is seen clearly in Fig. 7 which shows P, Q, and v vs τ at selected values of θ. The entire evolution is displayed in a three-dimensional (3D) surface plot in Figs. 8 (for P and Q) and 9 (for v and $v < 1$).

We note the following features of the evolution.

(1) The wave amplitude P develops a complicated spatial profile which then freezes after which P grows linearly without change of shape.

(2) The amplitude Q initially grows rapidly [where $\cos\theta < 0$ since there $P_{,\tau}$ in (3.3) acts as inverse damping] but then becomes constant. (There is some spatial struc-

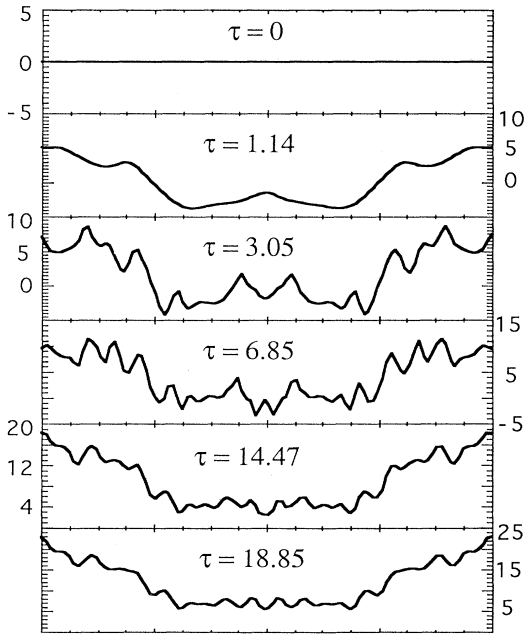

FIG. 4. $P(\theta,\tau)$ vs θ at selected values of τ. Results of the simulation for initial data from (5.1) in the fourth-order accurate numerical scheme are shown. The computation was performed with 800 spatial grid points. The display consists of values at 100 of these grid points averaged over nearest and next-nearest neighbors in the full array. (The selection of spatial grid points accounts for any asymmetry about $\theta = \pi$.) Six graphs at selected τ values are stacked. In all cases, the horizontal axis is $0 \le \theta \le 2\pi$. The numerical scales on either the left or right axis denote the amplitude of P. The simulation represents the range $0 \le \tau \le 18.85$.

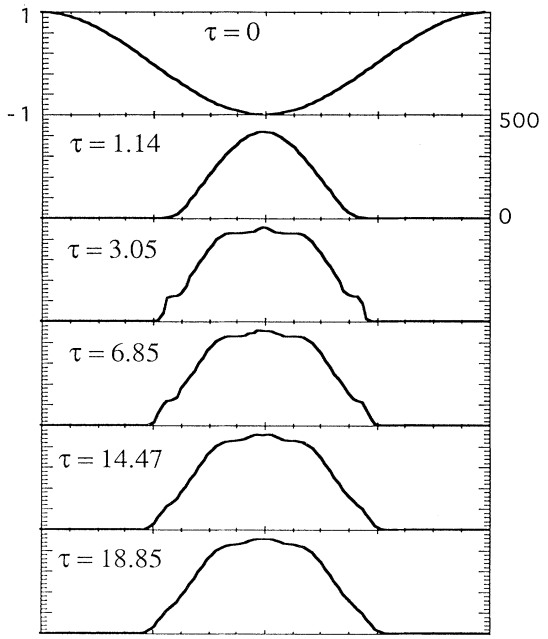

FIG. 5. $Q(\theta,\tau)$ vs θ at selected values of τ. The same as Fig. 4 but for Q. For $\tau \geq 1.14$, the vertical scale is [0,500].

ture in Q which does not show up for the amplitude scale used in this graph.)

(3) The parameter v decays essentially monotonically to values <1 everywhere. This is emphasized by Fig. 9(b) which has a scale adjusted to display only $v \leq 1$.

It thus appears that the AVTD regime has been reached and that the parameter v has fallen below unity

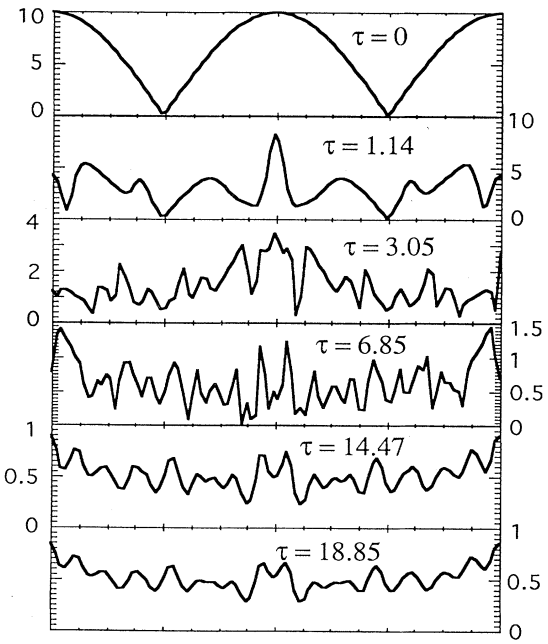

FIG. 6. $v(\theta,\tau)$ vs θ at selected values of τ. The same as Fig. 4 but for v as defined by (3.21).

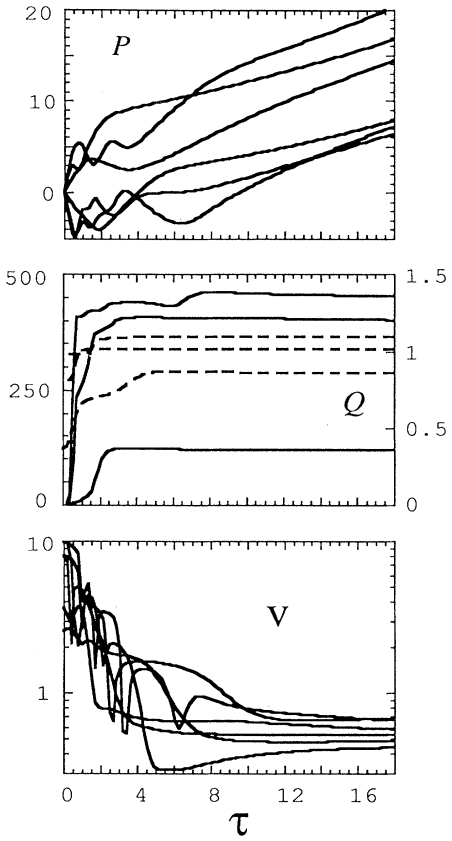

FIG. 7. $P(\theta,\tau)$, $Q(\theta,\tau)$, and $v(\theta,\tau)$ vs τ at selected values of θ. In all cases, the horizontal axis is $0 \leq \tau \leq 18$. On the graph for Q, the values of the solid lines correspond to the left axis and the dashed lines to the right axis.

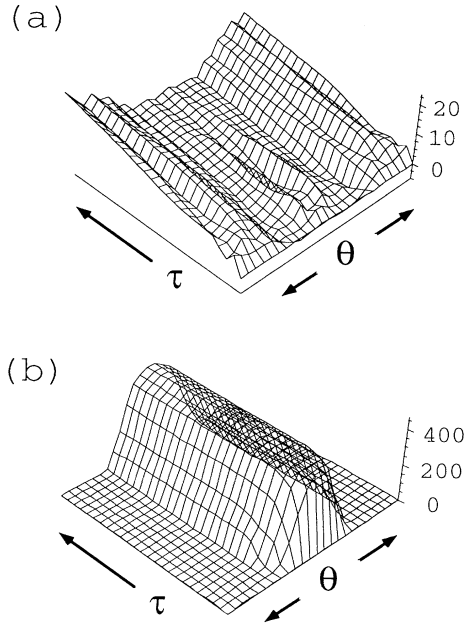

FIG. 8. P and Q in the θ-τ plane. The complete results of the simulation in Figs. 4–7 are shown in the θ-τ plane. The axis scales for θ and τ are $[0,2\pi]$ and $[0,6\pi]$, respectively. The vertical axes denote the values of (a) P and (b) Q, respectively.

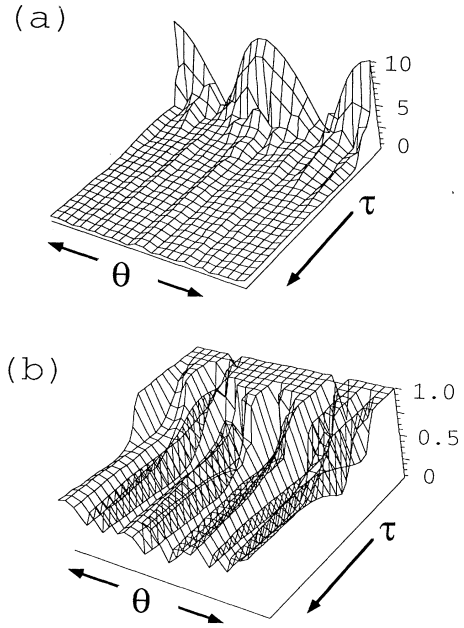

FIG. 9. The values of v in the θ-τ plane. This figure is the same as Fig. 8 but for the parameter v. Note that the viewing angle has changed for greater clarity. (a) All values of v. (b) The same data with the vertical scale chosen to display only $v \leq 1$.

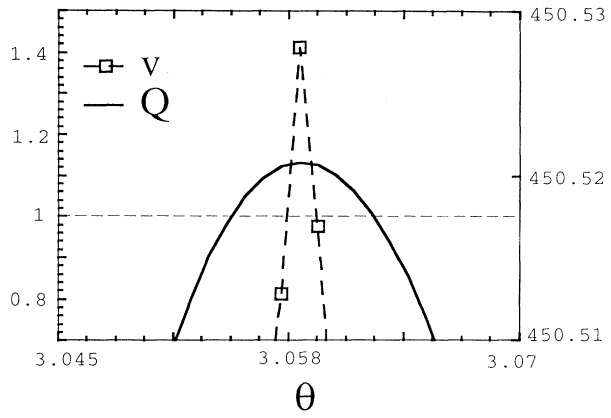

FIG. 10. A "nongeneric" point in θ. Q and v vs θ at $\tau=6\pi$ are shown near a point with $v>1$ for the initial data of Figs. 4–9 for a simulation with 6400 spatial grid points with no spatial averaging of the results. The graphs are produced using all the spatial resolution available in the simulation. The left axis corresponds to v and the right to Q. Note that $v>1$ only where $Q_{,\theta}\approx 0$ and that the ranges displayed for Q and θ are small. The horizontal dashed line denotes $v=1$.

as conjectured. Although we have begun with a single spatial mode, we expect the nonlinear terms to cause a generic evolution. Other standing wave initial data have been examined. It appears that the evolution is controlled to some extent by v_0, the initial value of the parameter v. If $v_0<1$, there is little growth of spatial structure and the AVTD regime is reached quickly. The larger v_0, the more nonlinear the wave interactions will be.

If spatial averaging is not used, $v>1$ can occur at isolated points where $Q_{,\theta}\approx 0$. (See Fig. 10.) Such points, in effect, represent the locally polarized models where $v\geq 1$ is allowed. To the extent that $Q_{,\theta}\neq 0$ (i.e., that the model really is generic at that point), it still evolves to reach the AVTD regime as conjectured at some $\tau\gg 6\pi$. The spatial averaging dilutes the influence of spiky features in the dynamical variables. The development of AVTD behavior with spatial averaging removed is shown in Fig. 11 where P/τ and v over a limited range in θ are shown for $\tau=6\pi$ and $\tau=14\pi$. The curves (at each τ value) should be identical in the AVTD limit as $\tau\rightarrow\infty$ [see (3.15)]. It appears that the asymptotic AVTD behavior will be achieved at sufficiently large τ.

The growth of spatial structure at arbitrarily small scales appears to be characteristic of the Gowdy T^3 dynamics for $v_0\geq 1$. Figure 12 reproduces Fig. 8(a) for $0\leq\tau\leq 4.2$. It is easy to see that the initial $\cos\theta$ spatial profile nonlinearly generates [through (3.2)] $\cos 2\theta$ dependence, etc. The development of this structure ends when the AVTD limit is reached. The competition between nonlinear growth and the spatial freezing of AVTD behavior suggests that there may exist a v_0-dependent time scale to characterize the phenomenon. It is possible that this small-scale structure may be related to the critical phenomena observed by Choptuik [33] and later by Abrahams and Evans [34] for spherical collapse of a scalar field and axisymmetric collapse of gravitational waves respectively.

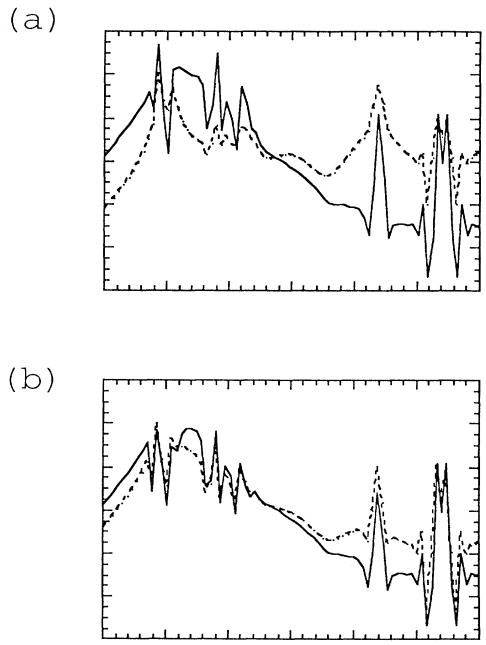

FIG. 11. Approaching the AVTD limit. Graphs of v (solid line) and P/τ (dashed line) vs θ are overlaid. The data are taken from the same simulation as Figs. 4–9 for 800 spatial grid points but with no spatial averaging. The vertical scale for both P/τ and v ranges from 0 to 1.2 while the horizontal axis is $2.6\leq\theta\leq 3.2$. (a) $\tau=18.86$; (b) $\tau=43.96$.

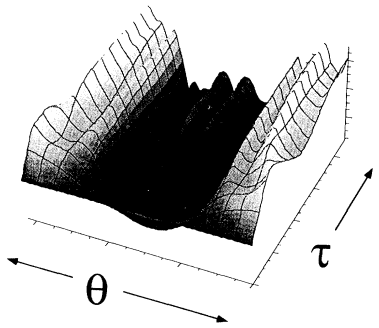

FIG. 12. Growth of small-scale spatial structure. The graph shows the data for $P(\theta,\tau)$ from Fig. 8(a) for the range $0\leq\tau\leq 4.2$.

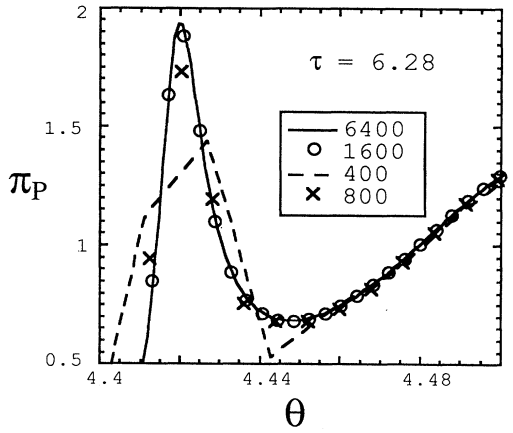

FIG. 13. Spatial resolution dependence of generic spiky features. A typical spiky feature in π_P vs θ at $\tau=2\pi$ is shown at resolutions of 400, 800, 1600, and 6400 spatial grid points.

The presence of this small-scale spatial structure which eventually reaches the grid spacing scale (unless the AVTD regime is reached) causes the detailed numerical evolution to become dependent on the chosen spatial resolution—i.e., at a given τ, the finer the grid, the smaller the feature that is seen. However, for any τ there exists a spatial resolution which is sufficient to resolve all the small scale features. This is shown (with no spatial averaging) in Fig. 13 which compares the same feature (in this case for π_P) at various spatial resolutions. We note that the feature is completely resolved at 6400 grid points with a profile that agrees completely with that obtained for 1600 grid points. Greater deviations are found for coarser grids. All resolutions represent the solution where it is smooth. The evolution of this same feature is shown in Fig. 14. We see that the feature has narrowed (and decreased in amplitude) and is no longer resolved at 6400 grid points. This narrowing and decreasing amplitude explains the apparent decrease in spatial structure seen in the evolution shown in Fig. 4 (although some is due to the increased range in the amplitude of P). The spatial averaging used in Figs. 4–9 washes out the structure at small spatial scales. Subsequent evolution of the feature in Fig. 14 shows little change, indicating that AVTD behavior (where $\pi_P\rightarrow$const) is arising.

This small-scale structure is almost certainly a real property of the equations rather than a numerical artifact since it can be resolved with sufficient spatial resolution. (As a further code test, the structure is seen to disappear when the code is run backward in time. It was also seen in studies of the approach to the singularity using a completely different numerical algorithm [35].) Its characterization is currently under investigation. Its presence may signal a requirement for adaptive gridding [36] to achieve the spatial resolution that appears to be necessary.

VI. THE U(1) PROBLEM

It has been shown [14] that an arbitrary cosmological spacetime on $T^3\times R$ containing a spacelike U(1) symmetry can be described by the 5 degrees of freedom φ, ω, x, z, Λ and their respective conjugate momenta p, r, p_x, p_z, p_Λ. All variables are functions of the spatial coordinates u and v and a time coordinate τ which measures the size of the universe in the symmetry direction. The conformal two-metric of the space orthogonal to the Killing field is

$$e_{ab}=\frac{1}{2}\begin{bmatrix} e^{2z}+e^{-2z}(1+x)^2 & e^{2z}+e^{-2z}(x^2-1) \\ e^{2z}+e^{-2z}(x^2-1) & e^{2z}+e^{-2z}(x-1)^2 \end{bmatrix} \tag{6.1}$$

with $a,b=1,2$ and $\det e_{ab}=1$. (The two-metric itself is $g_{ab}=e^{\Lambda}e_{ab}$.) The scalar curvature of this conformal two-space is

$$\begin{aligned} {}^{(2)}R(e_{ab})\equiv R=&[e^{-2z}(1-x)x_{,u}+e^{-2z}(1-x)^2z_{,u}-e^{2z}z_{,u}-e^{-2z}x_{,v}+e^{2z}z_{,v}+e^{-2z}z_{,v}+e^{-2z}xx_{,v}-e^{-2z}x^2z_{,v}]_{,u}\\ &+[-e^{-2z}(1+x)x_{,v}+e^{-2z}(1+x)^2z_{,v}-e^{2z}z_{,v}+e^{-2z}x_{,u}+e^{2z}z_{,u}+e^{-2z}z_{,u}+e^{-2z}xx_{,u}-e^{-2z}x^2z_{,u}]_{,v}\ . \end{aligned} \tag{6.2}$$

Given these definitions, the field equations (for the dynamical variables in the gauge $N=\sqrt{{}^2g}=e^{\Lambda}$, where N is the lapse and ${}^2g$ is the determinant of the two-metric) can be derived from the Hamiltonian

$$\begin{aligned} H=&-\oint\oint du\,dv(\tfrac{1}{8}p_z^2+\tfrac{1}{2}e^{4z}p_x^2+\tfrac{1}{8}p^2+\tfrac{1}{2}e^{4\varphi}r^2-\tfrac{1}{2}p_\Lambda^2-2p_\Lambda)\\ &-e^{-2\tau}\oint\oint du\,dv[-e^{\Lambda}R+e^{\Lambda}(e^{ab}\Lambda_{,a})_{,b}+2e^{\Lambda}e^{ab}\varphi_{,a}\varphi_{,b}+\tfrac{1}{2}e^{\Lambda}e^{-4\varphi}e^{ab}\omega_{,a}\omega_{,b}]\ . \end{aligned} \tag{6.3}$$

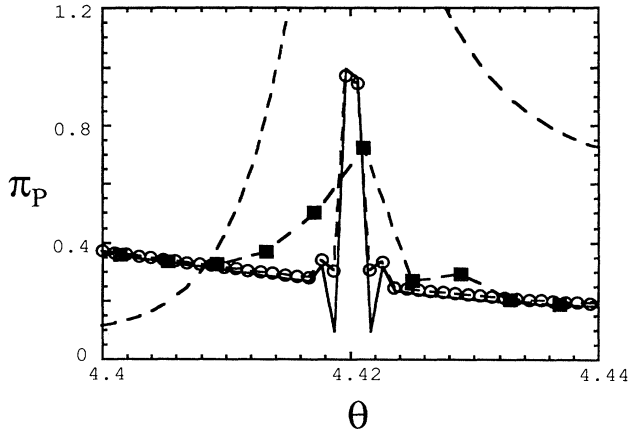

FIG. 14. Evolution of a spiky feature. The dashed line indicates the same plot as Fig. 13 at $\tau=2\pi$ for 6400 spatial grid points on the expanded scale of this figure. The same feature at 6400 spatial grid points is shown at $\tau=4\pi$ (solid line) and $\tau=6\pi$ (dashed line with circles). For comparison, the feature computed with 1600 spatial grid points is shown at $\tau=4\pi$ (dashed line with squares).

We note that the integrand in Eq. (6.3) is not the super-Hamiltonian, but differs from it by an overall sign and an additional term linear in p_Λ. The sign arises from the fact that τ results from an original time variable t via $dt=-e^{-\tau}d\tau$ while the additional term comes from the fact that a time-dependent transformation is required to obtain our variables from the original Arnowitt-Deser-Misner (ADM) [37] ones.

It is clear that the Hamiltonian (6.3) fits naturally into the form of the SI operator splitting. Even more striking is the fact that the first integral H_1 contains two copies of the Gowdy T^3 kinetic term [see (3.8)] plus the kinetic energy of a free particle (with the "wrong" sign). Thus, we already have the exact solution for H_1 from (3.12) and (3.13) as in the Gowdy case plus the trivial free particle solution. The second integral H_2 is more difficult—not to solve since there are no momenta so all the variables are assumed constant over the sub-time-step—but to spatially difference to the correct order of accuracy.

In addition, the dynamical degrees of freedom are constrained—the Gowdy split into wave and background variables does not occur. For example, the integrand of (6.3), leaving out the term linear in p_Λ, is proportional to the Hamiltonian constraint. There are also nontrivial momentum constraints. Since the same terms occur in H_2 and in the Hamiltonian constraint, it is probably advantageous to preserve the divergence structure of the first two terms in the square brackets rather than to partially integrate them. A differencing scheme for the field equations that recognizes the underlying structure of the constraints may aid in keeping the numerical evolution on the constraint hypersurface. Although the differencing scheme for H_2 outlined in Sec. II can be extended to the Laplacian, it becomes problematical for the mixed partial derivatives that will arise here. We plan to begin with a plausible second-order accurate scheme.

Since the dynamical evolution is constrained, specification of initial data is nontrivial. Fortunately, examples of "half-polarized" exact solutions of the constraint equations are known [38].

Although almost nothing is known about the generic behavior of the U(1) models, it is known that not all solutions can be AVTD. This is because this class of solutions contains the mixmaster cosmologies [2–4] which (since the influence of the potential never disappears) are not AVTD. If, as has been conjectured, the mixmaster dynamics cannot survive the presence of the spatial inhomogeneity degrees of freedom, the models could still be AVTD. We note here, however, that the transformation necessary to obtain our variables has obscured the meaning of AVTD since the transformation to the twist potential degree of freedom $[\omega,r]$ has interchanged coordinates and momenta. It is also expected that small-scale spatial structure will appear in the generic case. The possible need for high spatial resolution in two spatial dimensions may push the limits of current computational technology.

VII. SUMMARY AND CONCLUSIONS

A SI scheme that splits the Hamiltonian into exactly solvable kinetic and potential pieces is ideally suited to the numerical study of the singularity structure of spatially inhomogeneous cosmologies. For both the Gowdy T^3 model and the more general U(1) problem (on $T^3\times R$), the dynamical equations arise from a variational principle that also splits naturally into kinetic and potential pieces which separately can be solved exactly. The exact solution for the kinetic sub-Hamiltonian is, in fact, just the AVTD solution conjectured to arise for the generic Gowdy T^3 model [taken twice plus a free particle term in the U(1) problem].

The SI code has been implemented through fourth-order in both time (using Suzuki's method) and space for the generic Gowdy model. Comparison for a pseudounpolarized test case (obtained by a boost symmetry from an exact solution for the polarized model) shows agreement to $1{:}10^5$ for the fourth-order accurate code. The second-order accurate code diverges unacceptably in regions of large spatial derivative as the singularity is approached. The cost of the extra accuracy is essentially a factor of 3 in computational time (since three second-order time steps are required to produce a fourth-order time step). The extra spatial accuracy involves negligible cost.

For reasonably generic Gowdy initial data, we have been able to support the conjecture [13] that the models are AVTD with $v<1$ everywhere. A more detailed study of the approach to the AVTD regime to compare with the detailed predictions in [13] is in progress.

An interesting new phenomenon of the development of small-scale spatial structure has been observed. Studies to characterize this behavior in terms of the competition between nonlinear generation of short-wavelength modes and the freezing of the spatial profile in the AVTD regime are underway.

Thus, we have applied the SI scheme to the unpolarized Gowdy T^3 cosmology and have been able to test the

code, to study and verify the AVTD regime conjectures, and to discover the new phenomenon of nonlinear small-scale structure. An even richer phenomenology awaits the application of this method to the unknown territory of the U(1) problem.

ACKNOWLEDGMENTS

This research was supported in part by NSF Grant Nos. PHY89-04035 to the Institute for Theoretical Physics, University of California/Santa Barbara, PHY91-07162 to Oakland University, and PHY92-01196 to Yale University. Computations were performed using the facilities of the National Center for Supercomputing Applications at the University of Illinois. B.K.B. wishes to thank the Institute for Geophysics and Planetary Physics at Lawrence Livermore National Laboratory for hospitality. The authors wish to thank Boro Grubišić, David Garfinkle, and Salman Habib for useful discussions.

APPENDIX: DETAILS OF THE SECOND-ORDER ACCURATE SI ALGORITHM FOR THE GOWDY T^3 MODEL

The Hamiltonian (3.8) can be put in differenced form

$$H=\sum_{i=0}^{N}\tfrac{1}{2}(\pi_{P_i}^2+e^{-2P_i}\pi_{Q_i}^2)+\sum_{i=0}^{N}\tfrac{1}{2}e^{-2\tau}\left[\left[\frac{P_{i+1}-P_i}{\Delta\theta}\right]^2+e^{P_{i+1}+P_i}\left[\frac{Q_{i+1}-Q_i}{\Delta\theta}\right]^2\right] \tag{A1}$$

with each sum regarded to be an independent sub-Hamiltonian (H_1 and H_2, respectively). Given initial data $Q_i(\tau^j)$, $P_i(\tau^j)$, $\pi_{Q_i}(\tau^j)$, $\pi_{P_i}(\tau^j)$, we use H_2 to evolve to $\tau^j+\frac{1}{2}\Delta\tau$ to yield

$$\begin{aligned}
&\tilde{Q}_i=Q_i(\tau^j)\ ,\\
&\tilde{P}_i=P_i(\tau^j)\ ,\\
&\tilde{\pi}_{Q_i}=\pi_{Q_i}(\tau^j)+\tfrac{1}{2}e^{-2\tau_j}[e^{-(\tau_{j+1}-\tau_j)}-1]\frac{\partial V}{\partial Q_i}\bigg|_{Q_k(\tau^j),P_k(\tau^j)}\ ,\\
&\tilde{\pi}_{P_i}=\pi_{P_i}(\tau^j)+\tfrac{1}{2}e^{-2\tau_j}[e^{-(\tau_{j+1}-\tau_j)}-1]\frac{\partial V}{\partial P_i}\bigg|_{Q_k(\tau^j),P_k(\tau^j)}\ ,
\end{aligned} \tag{A2}$$

where V is the "spatially dependent" part of the potential term in (A1). Note that the time dependence has been taken into account separately and that two terms in the sum contribute to the indicated gradient.

Now solve the AVTD equations (3.12) and (3.13) and their τ derivatives using $\tilde{Q}_i$, $\tilde{P}_i$, $\tilde{\pi}_{Q_i}$, $\tilde{\pi}_{P_i}$ for the constants ζ_i, β_i, α_i, and ξ_i. We find the following.

(1) If $\tilde{\pi}_{P_i}\neq 0$ *and* $\tilde{\pi}_{Q_i}\neq 0$ then

$$\zeta_i=\frac{-1+[1+(\tilde{\pi}_{Q_i}e^{-\tilde{P}_i}/\tilde{\pi}_{P_i})^2]^{1/2}}{(\tilde{\pi}_{Q_i}e^{-\tilde{P}}/\tilde{\pi}_{P_i})}\ , \tag{A3a}$$

$$\beta_i=\left[\frac{1+\zeta_i^2}{\zeta_i^2-1}\right]\tilde{\pi}_{P_i}\ , \tag{A3b}$$

$$\alpha_i=\frac{e^{\tilde{P}_i}}{1+\zeta_i^2}\ , \tag{A3c}$$

$$\xi_i=\tilde{Q}_i+\zeta_i e^{-\tilde{P}_i}\ . \tag{A3d}$$

(2) If $\tilde{\pi}_{P_i}\neq 0$ *but* $\tilde{\pi}_{Q_i}=0$ then

$$\zeta_i=0,\quad \beta_i=-\tilde{\pi}_{P_i},\quad \alpha_i=e^{\tilde{P}_i},\quad \xi_i=\tilde{Q}_i\ . \tag{A4}$$

(3) If $\tilde{\pi}_{P_i}=0$ then for any $\tilde{\pi}_{Q_i}$,

$$\begin{aligned}
&\zeta_i=1,\quad \beta_i=-\tilde{\pi}_{Q_i}e^{-\tilde{P}_i}\ ,\\
&\alpha_i=\tfrac{1}{2}e^{\tilde{P}_i},\quad \xi_i=\tilde{Q}_i+e^{-\tilde{P}_i}\ .
\end{aligned} \tag{A5}$$

These values are then used to evolve $\tilde{Q}_i$, $\tilde{P}_i$, $\tilde{\pi}_{Q_i}$, $\tilde{\pi}_{P_i}$ with the AVTD equations to $\tau^j+\Delta\tau$. This is just the evolution by H_1 required by the algorithm. We find

$$\tilde{\tilde{\pi}}_{Q_i}=\tilde{\pi}_{Q_i}\ , \tag{A6a}$$

$$\tilde{\tilde{\pi}}_{P_i}=-\frac{\beta_i(e^{-\beta_i(\tau_{j+1}-\tau_j)}-\zeta_i^2e^{\beta_i(\tau_{j+1}-\tau_j)})}{e^{-\beta_i(\tau_{j+1}-\tau_j)}+\zeta_i^2e^{\beta_i(\tau_{j+1}-\tau_j)}}\ , \tag{A6b}$$

$$\tilde{\tilde{P}}_i=\ln[\alpha_i(e^{-\beta_i(\tau_{j+1}-\tau_j)}+\zeta_i^2e^{\beta_i(\tau_{j+1}-\tau_j)})]\ , \tag{A6c}$$

$$\tilde{\tilde{Q}}_i=\xi_i-\left[\frac{\zeta_i e^{2\beta_i(\tau_{j+1}-\tau_j)}}{\alpha_i(1+\zeta_i^2e^{2\beta_i(\tau_{j+1}-\tau_j)})}\right]\ . \tag{A6d}$$

Finally, $\tilde{\tilde{Q}}_i$, $\tilde{\tilde{P}}_i$, $\tilde{\tilde{\pi}}_{Q_i}$, $\tilde{\tilde{\pi}}_{P_i}$ are evolved with H_2 for $\Delta\tau/2$ to yield the original variables updated to the next time step:

$$\begin{aligned}
&Q_i(\tau^{j+1})=\tilde{\tilde{Q}}_i\ ,\\
&P_i(\tau^{j+1})=\tilde{\tilde{P}}_i\ ,\\
&\pi_{Q_i}(\tau^{j+1})=\tilde{\tilde{\pi}}_{Q_i}+\tfrac{1}{2}e^{-(\tau_{j+1}+\tau_j)}[e^{-(\tau_{j+1}-\tau_j)}-1]\frac{\partial V}{\partial Q_i}\bigg|_{\tilde{\tilde{Q}}_k,\tilde{\tilde{P}}_k}\ ,\\
&\pi_{P_i}(\tau^{j+1})=\tilde{\tilde{\pi}}_{P_i}+\tfrac{1}{2}e^{-(\tau_{j+1}+\tau_j)}[e^{-(\tau_{j+1}-\tau_j)}-1]\frac{\partial V}{\partial P_i}\bigg|_{\tilde{\tilde{Q}}_k,\tilde{\tilde{P}}_k}\ .
\end{aligned} \tag{A7}$$

To achieve fourth-order accuracy in time, repeat the entire procedure three times with steps of $s\Delta\tau$, $(1-2s)\Delta\tau$, and $s\Delta\tau$, respectively, with $s=(2-2^{1/3})^{-1}$. For fourth-order spatial accuracy, replace the potential term in (A1) by the appropriate version of (4.1).

[1] R. Penrose, Phys. Rev. Lett. **14**, 57 (1965); S. W. Hawking, Proc. R. Soc. London **A300**, 187 (1967); S. W. Hawking and R. Penrose, *ibid.* **A314**, 529 (1970); see also S. W. Hawking and G. F. R. Ellis, *The Large Scale Structure of Space-Time* (Cambridge University Press, Cambridge, England, 1973); R. M. Wald, *General Relativity* (University of Chicago, Chicago, 1984).

[2] V. A. Belinskii and I. M. Khalatnikov, Zh. Eksp. Teor. Fiz. **56**, 1700 (1969) [Sov. Phys. JETP **29**, 911 (1969)]; **57**, 2163 (1969) [**30**, 1174 (1969)]; **59**, 314 (1971) [**32**, 169 (1971)]; V. A. Belinskii, I. M. Khalatnikov, and E. M. Lifshitz, Adv. Phys. **19**, 525 (1970); **31**, 639 (1982); V. A. Belinskii, E. M. Lifshitz, and I. M. Khalatnikov, Usp. Fiz. Nauk. **102**, 463 (1971) [Sov. Phys. Usp. **13**, 745 (1971)].

[3] I. M. Khalatnikov and V. L. Pokrovski, in *Magic Without Magic,* edited by J. Klauder (Freeman, San Francisco, 1972), p. 441.

[4] C. W. Misner, Phys. Rev. Lett. **22**, 1071 (1969); in *Relativity,* edited by M. Carmeli *et al.* (Plenum, New York, 1970), p. 55; in *Magic Without Magic* [3], p. 441.

[5] See M. MacCallum, in *General Relativity, an Einstein Centenary Survey,* edited by S. W. Hawking and W. Israel (Cambridge University Press, Cambridge, 1979); R. T. Jantzen, in *Cosmology of the Early Universe,* edited by R. Ruffini and L. Z. Fang (World Scientific, Singapore, 1984), p. 233.

[6] See J. D. Barrow and F. Tipler, Phys. Rep. **56**, 372 (1979).

[7] P. Halpern, Gen. Relativ. Gravit. **19**, 73 (1987); R. M. Wald and A. Higuchi (private communication); H. Ishihara, Prog. Theor. Phys. **74**, 490 (1985). Note that a rotational degree of freedom provides a counterexample [see M. P. Ryan, Jr., Ann. Phys. (N.Y.) **65**, 506 (1971); M. P. Ryan, Jr. and L. C. Shepley, *Homogeneous Relativistic Cosmologies* (Princeton University, Princeton, 1975)].

[8] D. Eardley, E. Liang, and R. Sachs, J. Math. Phys. **13**, 99 (1972).

[9] J. Isenberg and V. Moncrief, Ann. Phys. (N.Y.) **199**, 84 (1990).

[10] R. H. Gowdy, Phys. Rev. Lett. **27**, 826 (1971); **27**, E1102 (1971); Ann. Phys. (N.Y.) **83**, 203 (1974).

[11] P. T. Chrusciel, J. Isenberg, and V. Moncrief, Class. Quantum Grav. **7**, 1671 (1990).

[12] B. K. Berger, Ann. Phys. (N.Y.) **83**, 458 (1974).

[13] B. Grubišić and V. Moncrief, Phys. Rev. D **47**, 2371 (1993).

[14] V. Moncrief, Ann. Phys. (N.Y.) **167**, 118 (1986).

[15] J. Eells and J. Sampson, Am. J. Math. **86**, 109 (1964); C. Misner, Phys. Rev. D **18**, 4510 (1978).

[16] V. Moncrief, Ann. Phys. (N.Y.). **132**, 87 (1981).

[17] J. A. Fleck, J. R. Morris, and M. D. Feit, Appl. Phys. **10**, 129 (1976); V. Moncrief, Phys. Rev. D **28**, 2485 (1983).

[18] B. K. Berger, D. Garfinkle, and V. Moncrief (unpublished).

[19] J. Centrella and R. A. Matzner, Astrophys. J. **230**, 311 (1979); Phys. Rev. D **25**, 930 (1982); P. Anninos, J. Centrella, and R. A. Matzner, *ibid.* **39**, 2155 (1989); **43**, 1808 (1991); **43**, 1825 (1991).

[20] See *Frontiers in Numerical Relativity,* edited by C. R. Evans, L. S. Finn, and D. W. Hobill (Cambridge University Press, Cambridge, 1989).

[21] M. Suzuki, Phys. Lett. A **146**, 319 (1990); J. Math. Phys. **32**, 400 (1991).

[22] M. P. Ryan, Jr., in *Relativity and Gravitation: Classical and Quantum,* Proceedings of SILARG VII, Cocoyoc, Mexico, 1990, edited by J. C. D'Olivo *et al.* (World Scientific, Singapore, 1991), pp. 96–121.

[23] W. H. Press, B. P. Flannery, S. A. Teukolsky, and W. T. Vetterling, *Numerical Recipes in* FORTRAN*: The Art of Scientific Computing,* 2nd ed. (Cambridge University Press, Cambridge, 1992); C. A. Hall and T. A. Porsching, *Numerical Analysis of Partial Differential Equations* (Prentice Hall, Englewood Cliffs, NJ, 1990); A. R. Mitchell and D. F. Griffiths, *The Finite Difference Method in Partial Differential Equations* (Wiley, New York, 1980).

[24] R. Ove, Ph.D. thesis, Yale University, 1985.

[25] B. K. Berger, Ann. Phys. (N.Y.) **156**, 155 (1984).

[26] E. Kasner, Am. J. Math. **43**, 130 (1921).

[27] R. A. Isaacson, Phys. Rev. **166**, 1263 (1968); **166**, 1272 (1968).

[28] D. R. Brill and J. B. Hartle, Phys. Rev. **135**, B271 (1964).

[29] This was noticed numerically by David Garfinkle (private communication).

[30] One can show that the spacetimes discussed by V. Moncrief [Ann. Phys. (N.Y.) **141**, 83 (1982)], restricted to the Gowdy class, have this property. For a more complete treatment of this question see P. Mansfield, Ph.D. thesis, Yale University, 1989.

[31] The exact solutions were computed using Bessel function subroutines given in W. H. Press, B. P. Flannery, S. A. Teukolsky, and W. T. Vetterling, *Numerical Recipes in* FORTRAN*: The Art of Scientific Computing* [23].

[32] P. Chrusciel (private communication).

[33] M. W. Choptuik, Phys. Rev. Lett. **70**, 9 (1993).

[34] A. M. Abrahams and C. R. Evans, Phys. Rev. Lett. **70**, 2980 (1993).

[35] C. M. Swift, Masters thesis, Oakland University, 1992; B. K. Berger, D. Garfinkle, and C. M. Swift (unpublished).

[36] See the discussion of adaptive gridding in [33] and references therein.

[37] R. Arnowitt, S. Deser, and C. W. Misner, in *Gravitation: An Introduction to Current Research,* edited by L. Witten (Wiley, New York, 1962), p. 227.

[38] V. Moncrief (unpublished).

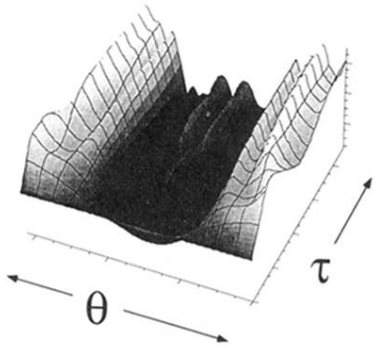

FIG. 12. Growth of small-scale spatial structure. The graph shows the data for $P(\theta,\tau)$ from Fig. 8(a) for the range $0 \leq \tau \leq 4.2$.